Investigation of apparent correlated motion of Brownian particles

Richard V. Durand and Carl Franck
Laboratory of Atomic and Solid State Physics and Materials Science Center, Cornell University, Ithaca, New York 14853-2501
(Received 15 November 1996; revised manuscript received 14 April 1997)

We, as well as other workers, have noticed using light microscopy that particles undergoing Brownian motion can appear to linger around each other for long periods of time. The question arises as to whether this lingering is a product of interparticle interactions, or is an artifact due to random thermal motion and projection onto a two-dimensional image plane. To answer this question, we produced digitized animations of colloidal particles using light microscopy images of a system composed of micrometer-sized latex spheres suspended in water. Six observers, unfamiliar with the experiment, watched these animations for lingering among the particles. Control animations were also generated from these data sets in which correlations due to particle-particle interactions had been destroyed, but the probability of the aforementioned artifactual correlations remained unchanged. We found that the differences in what people observed in the real and control data were not statistically significant. Thus, we conclude that any lingering observed on the time scale of 10 s and the length scale of 5 μm is the result of the random motion of the particles and projection effects. By way of explaining this result theoretically, we find that on this length and time scale, hydrodynamic interactions dominate over electrostatic and van der Waals forces. Accordingly, we present numerical and analytical calculations of the enhanced lingering associated with the decrease in hydrodynamic mobility of closely separated particles. These calculations give results which are consistent with the conclusion that the enhanced lingering effect is too small to be seen by an individual observer. [S1063-651X(97)13908-3]

PACS number(s): 82.70.Dd, 07.05.Rm, 05.40.+j, 47.90.+a

I. INTRODUCTION

While viewing dilute colloidal suspensions through a microscope, we, along with other workers [1–3], have noticed that particles occasionally appear to linger around each other for unusual lengths of time while undergoing Brownian motion. Cheung *et al.*, during the study of a colloidal system confined to a soap film, actually observed pairs of particles swirling around each other, a motion they likened to ''square dancing'' [3]. The traditional physics approach would be to take these observations as an interesting sign of correlated motion, and attempt to develop an entirely objective measure of the lingering effect. This measure could then, for example, be coded into a computer, which could then analyze many hours of digitized microscopy data in the search for examples of this lingering phenomenon. Cheung *et al.* actually employed this approach, choosing the two-particle relative diffusion tensor as their lingering measure [3].

While the traditional approach yields information about the actual interactions present in the system, it has no bearing on the initial inspirational observations, as it does not answer the question: are people actually observing correlations due to particle-particle interactions, or are the apparent correlations only due to perception based artifacts [4]? Random thermal encounters could be responsible for keeping two particles near each other for long periods of time. In addition, particles that appear close in an image may in fact be widely separated, because, in light microscopy, one typically projects a three-dimensional region onto a two-dimensional image plane. These projection effects could be responsible for some of the lingering of particles.

In this work, we attempted to answer this question directly by presenting naive observers with animated movies of micrometer-sized polystyrene spheres undergoing Brownian motion in water; half of these animations were representations of real data, while the remainder of the animations were composed of reference data in which nonartifactual correlations between particles had been removed by a scrambling procedure. Schirato and Franck found that in a pure simulation of a colloidal system, such reference data enabled efficient detection of correlated motion [5]. Our observers were not told about the different types of data sets, but were only asked to find ''lingering'' events between particles. We examined their responses without knowledge of the nature of the data sets, thereby providing a double blind study. After taking into account differences in particle density between the movies, it was found that no more lingering events were noticed in the real data than in the scrambled, or reference, data. Numerical and analytical estimates of a lingering effect due to quasistatic hydrodynamic interactions are consistent with this conclusion.

In Sec. II, we discuss the Brownian colloidal system and the steps involved in transforming the visual image in the microscope into the animated movies the observers actually saw. This includes digital image processing, particle tracking, and the generation of randomized data sets. The observer methodology is also discussed.

In Sec. III, the results of the experiment are presented. We define a statistic that scales away individual observer biases to give a measure of the particle interaction strength. This allows us to make quantitative estimates of the expected results.

In Sec. IV, we show that on the length and time scales relevant to our system, particle-particle hydrodynamic interactions dominate over other forces, and we estimate the interaction strength using computer simulations and analytical approximations. The Langevin equation is solved numerically with and without pairwise hydrodynamic interactions

present. A perturbation technique is developed for finding an approximate analytical solution to the diffusion equation including hydrodynamic interactions. We compare the numerical and analytical results with the results of Sec. III. Previous studies that used dynamical information to investigate colloidal interactions did not include this hydrodynamic contribution [6–8] (which, we feel, in principle, should be included). Cheung *et al.* believed hydrodynamic interactions to be responsible for the anomalous particle lingering in their two-dimensional system, but proposed no quantitative theories to explain it [3].

II. EXPERIMENTAL DESIGN

A. Sample

The charge stabilized latex particles used in this work were provided by Central Scientific (stock number 72704.11) [9]. They had a diameter of 1.054 μm, and were shipped in a 1.5% volume fraction solution. We used a colloidal suspension consisting of one drop of this solution diluted in 5-ml deionized water [1]. This yielded an estimated volume fraction of $\phi = 0.0005$. The Einstein-Stokes relation $D_0 = kT/6\pi\eta a$ [10] gives the free-particle diffusion coefficient $D_0 = 0.41\ \mu\text{m}^2/\text{s}$, where T is the temperature, η is the fluid viscosity, and a is the particle radius.

The sample cell was constructed by adhering two standard cover slips flat on a microscope slide using vacuum grease such that their inner edges were approximately parallel. Several drops of the diluted colloidal system were put in this rectangular well, and a third cover slip was placed on top to close the system. The openings in the sides were plugged with vacuum grease. The height of the sample cell is then the width of a cover slip, approximately 220 μm, and the width and length of the cell are approximately that of the top cover slip, or $1 \times 1\ \text{cm}^2$.

B. Digital imaging

The sample was viewed under an Olympus IMT-2 phase contrast microscope, and the particles were imaged using a video camera and recorded with a video cassette recorder (VCR). An Analogic frame capture card installed in a personal computer was then used to digitally capture frames from the videotape at the rate of 7.4 frames/s. This was the fastest rate achievable due to limitations of the VCR and controlling software [11]. Because the frame capture is field based, each frame is composed of an odd line field and an even line field interlaced together, taken $\frac{1}{60}$ s apart, yielding a total frame rate of 30 frames/s. In $\frac{1}{60}$ of a second, the particles will move about 0.16 μm in the x-y plane, or a sixth of the particle diameter, so the interlacing is not expected to cause significant distortion of the image.

A total of 208 s of video was digitized, which corresponds to 1538 frames. The raw images are in eight-bit gray-scale tagged image file format (TIFF) format, and have dimension 400×400 pixels, which corresponds to $118.0 \times 114.8\ \mu\text{m}^2$ in real space [12]. An example of a captured frame is shown in Fig. 1. The bright spots correspond to the particles. The images were manipulated using a software package called VISIONX [13], which was developed at Cornell University by A. Reeves *et al.*; VISIONX consists of a large collection of image processing tools and C library functions.

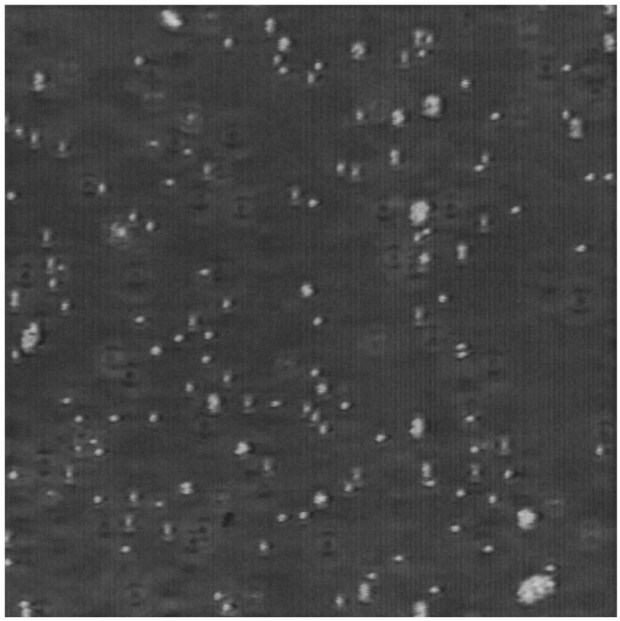

FIG. 1. A frame of digitized video before image processing. The image has dimension $118.0 \times 114.8\ \mu\text{m}^2$. The particles are represented by localized regions of high intensity.

The simplest method for extracting the particles from the images involves thresholding the images such that the particle features are retained, but any artifactual features in the background are suppressed. However, the presence of low spatial frequency light in the background with intensity close to that of the particles themselves makes it difficult to choose the optimal thresholding level. We chose the threshold level using a method that treats edges in the image as the most important features. This technique is as follows. First, we applied a Sobel edge detector to the images [14]. The magnitude of the edge detector function is a measure of the strength, or quality, of the edge. This gives an edge map for each image. Next, the original images were thresholded at gray levels ranging from 0 to 255, resulting in a series of binary images. In these binary images, we defined an edge to be any pixel having a different valued nearest neighbor pixel. This procedure results in an independent set of edge maps. The threshold figure of merit (TFOM) is defined as the magnitude of the Sobel edge operator averaged over the pixels where these two edge maps coincide [15]. A high TFOM indicates that the edges found by the Sobel algorithm and by the thresholding operation are similar. Thus, there are 255 TFOM's for each image, one for each possible thresholding level. For all the images, a plot of the TFOM versus thresholding level exhibited a wide plateau at a gray level of about 160, so each image was thresholded at this gray level to produce a binary image. A frame of video after this processing is shown in Fig. 2. These binary images were then segmented into regions of ''on'' and ''off'' pixels, and the coordinates of the center of mass of each of the connected regions of ''on'' pixels were recorded. These were interpreted as the coordinates of the particles in the images.

This procedure sets the depth of field h to $10.7 \pm 2.7\ \mu$m, which was determined by moving the focal plane of the microscope through particles that had adhered to the top cover

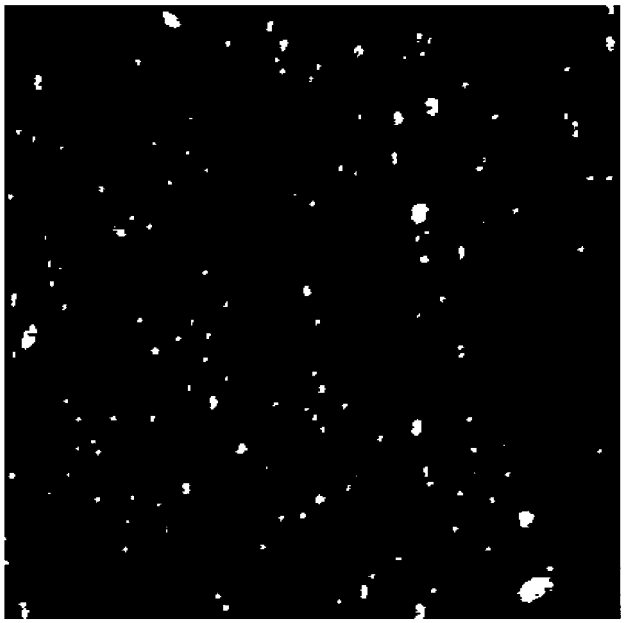

FIG. 2. The digitized frame of video in Fig. 1 after image processing.

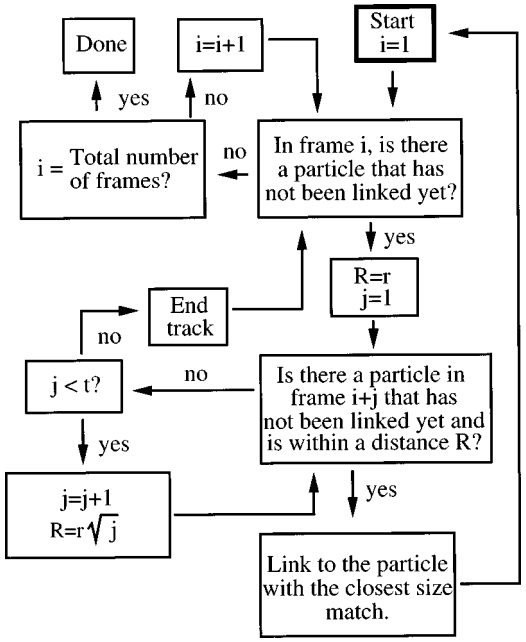

FIG. 3. Flow diagram of the tracking algorithm. The ''linking'' of particles indicated in the diagram refers to the process of linking particles in different frames together to form trajectories.

slip. Images taken at different depths were digitized, and processed as described above. Since after image processing the particles are either ''on'' or ''off,'' the depth of field was easily determined. Section II C will describe how these coordinates were linked together to form tracks.

C. Particle tracking

Particles undergoing random motion are particularly difficult to track. This is due to the lack of velocity or acceleration correlation from one frame to the next. The only information available to track one particle from frame to frame is the location and size of the particle. Recently, there has been great interest in using digital microscopy data to track Brownian particles in order to learn about various types of particle interactions [1,3,6–8,16]. However, most of the relevant papers give no details of the particular tracking algorithm used, with a notable exception being a recent paper by Crocker and Grier [8]. Thus we give a detailed description of our tracking algorithm here.

The tracking software attempts to link particles that are spaced closely in space and time and are similar in size. It accepts two user-defined parameters: r, which specifies the search region in spatial coordinates, and t, which specifies how far out in time we should search. A flow diagram is shown in Fig. 3. The spatial search radius can sometimes extend past the original value r for the following reason. If a particle drops out of the field of focus for a few frames, then, when it eventually comes back into view, it will likely be further away from its initial position than if it had still been in the field of focus in the subsequent frame. The growth of the spatial search radius as the square root of the number of skipped frames reflects the diffusive behavior of the particles.

The result from the above algorithm is a set of coordinates for each particle as a function of time. During our visual inspection of the inspirational colloidal video data, we found that we tended to focus our attention on the interactions between individual particles, and ignored any aggregates. We assumed that other workers noticing this lingering effect have also limited their attention to single particles. We wanted the system to appear to our observers as it appeared to us originally, and, thus, since many of the tracked objects are actually aggregates of particles, steps must be taken to eliminate these aggregates' tracks. One possibility is to allow only those tracks for which the particle's size stays within certain size bounds during its entire lifetime. However, size fluctuations along a particle's track would not be handled well by such a thresholding operation. If the size bounds were made too large, some aggregate tracks could be allowed, and, if the bounds were too small, then a particularly large size fluctuation could eliminate a valid single particle track. The solution to this problem is to ''soften'' the threshold by the introduction of hysteresis as follows. The first stage of the filtering process allows only those tracks which are likely to be associated with single particles. Along such tracks, a particle will have, at least at one point along its lifetime, a size close to the ''optimal'' size of a particle. Once these tracks are identified, a further size cut is made, where we reduce the effect of fluctuations by using much more relaxed size bounds than in the first cut. A track will pass this second cut if the particle satisfies these relaxed size bounds at all points in its lifetime. The numerical factor by which the optimal upper and lower size bounds are increased and decreased respectively in order to compute these relaxed bounds is called the ''hysteresis coefficient.'' For example, a hysteresis coefficient of 2.0 would mean that the particle's size would have to satisfy the optimal size bounds for at least one frame, and be greater than one-half the optimal lower size bound and less than twice the optimal upper size bound at all times. The tracking software allowed the specification of the optimal upper and lower diameter bounds, as well as the hysteresis coefficient [17].

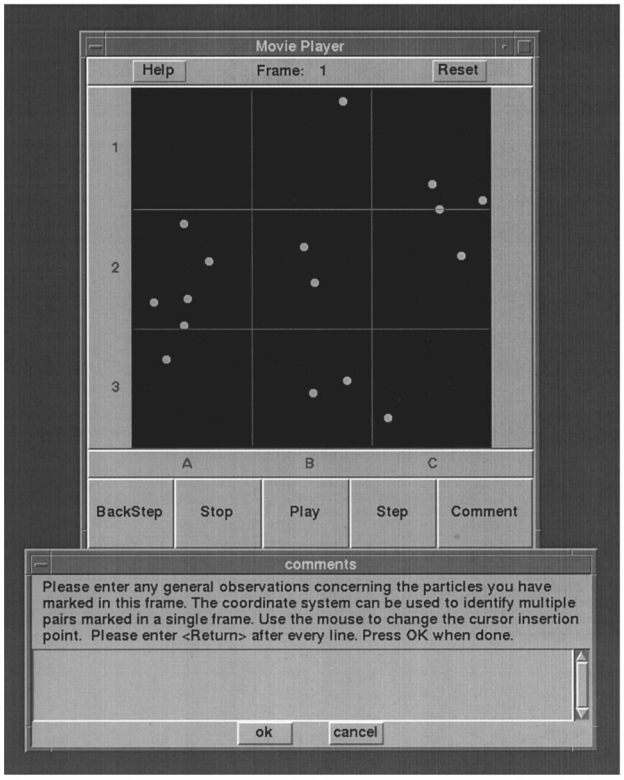

FIG. 4. A screenshot of the animated movie player. The frame shown is the same as in Figs. 1 and 2, but magnified by a factor 2 as described later in the text. Note that only the particles that pass through the discussed size filter appear. The 3×3 grid only appears when the observers make comments, and disappears while the movie is playing.

The appropriate optimal upper and lower bounds on the particles' size were determined by visual inspection of the images and from the distribution of particle sizes. A particle in the focal plane of the microscope has a diameter of about four pixels. This diameter can increase or decrease somewhat due to various optical artifacts that occur when the particle is slightly above or below the focal plane. Thus the low- and high-diameter cutoffs were set to one pixel and six pixels, respectively. The hysteresis coefficient was set equal to 2.0, because, if two particles happened to pass over one another, it would appear in the two-dimensional image as a collision of two particles, and the software would treat it as one large particle of twice the size of a single particle. Using this value of the hysteresis coefficient ensures that the size bounds will not be violated if this occurs.

In order to transform the coordinates of the particles into animated movies of Brownian motion, we developed a tool called the animated movie player (AMP). This software was written in a combination of Tcl/Tk and C on a RS/6000 running AIX 3.2. A screenshot is shown in Fig. 4. The AMP has standard features: play, rewind, frame step advance, and frame step reverse. The particles are represented as filled circles with a diameter consistent with the scale in the original image. There is also added functionality to enable the user to flag particles in the movie and make comments about them. The observers in the experiment used this software to watch the digitized sequences of images. We adjusted the frame rate in these animations to coincide with the frame rate of the video data on which they were based.

D. Generation of reference data sets

Three groups of 350 frames were extracted from the original data set, as it was found in preliminary trials with members of our research group that this was about the limit of a person's patience. Control, or reference, data sets were created by treating each particle's track as if it were a rigid two-dimensional wire, and then randomly translating and rotating it to a new position. This procedure destroys any correlated motion due to particle-particle interactions, but leaves intact apparent correlated motion due to random thermal encounters and projection effects. This was done for each of the three original data sets, and yielded three reference data sets. In order to eliminate any boundary effects of the randomization method, and reduce the total number of particles on screen to the more manageable level of about ten particles per frame, the center 200×200 pixel section of each of the six total data sets was extracted. The length scales in these data sets were subsequently increased by a factor of 2 to bring the size back up to 400×400 pixels, as this was a pleasant size for viewing.

In preliminary work, it was found that choosing certain values for the adjustable parameters r and t in the tracking algorithm resulted in particles being frequently misidentified. When an identification error exists, the algorithm used to create the reference sets will treat what should be one particle's track as two or more different tracks, and will split up the continuous track into multiple tracks scattered over the viewing area. Thus, upon viewing with the AMP, the reference data appear more discontinuous than the original data. Therefore, the parameters r and t used in the tracking algorithm were chosen empirically so as to minimize approximately the visual differences between the real and randomized data. The values $r=6$ and $t=6$ were found to give satisfactory results.

E. Observer methodology

Six observers were used in the experiment, all of whom were graduate students in physics at Cornell University. Great care was taken to ensure that they had no prior knowledge of any details of the experiment. Each was brought in individually, and was presented with three real and three reference movies in a random order, but the observers had no way of knowing if they were looking at real or reference data. They were allotted 5 min to view each movie and make comments. The work was completed in a single day to eliminate the possibility of communication about the experiment among the observers. The only guidelines as to what they should be looking for was contained in the following paragraph.

Objective: To watch the ''movie'' of the particles undergoing Brownian motion, and take note of any particles that seem to be ''lingering'' around each other for an unusually long time, or any other interesting behavior.

After each observer finished, he or she was asked if there were any problems with the software during the run. None of the observers reported any difficulties.

TABLE I. Number of lingering events scored by RD and CF for each observer and data set. The first number in each entry is RD's scoring, the second is CF's scoring. Discrepancies are discussed in the notes at the bottom.

	Frames 1–350		Frames 351–700		Frames 701–1050	
Observer	Original	Reference	Original	Reference	Original	Reference
1	1/1	3/3	0/0	0/0	1/1	3/3
2	2/2	3/3	1/1	1/1	1/1	4/4
3	3/1[a]	2/2	1/0[a]	2/2	2/1[b]	1/1
4	2/2	5/5	1/2[c]	4/3[d]	3/3	2/2
5[e]						
6[e]						

[a]The phrase ''fused together'' was used in some of the comments. RD counted these as events, CF did not.
[b]Only one particle was marked in one of the comments, but the wording of the comments suggested that the observer simply forgot to mark one of the particles. RD counted this as an event, CF did not.
[c]One of the comments was that the distance between a pair of particles ''grows steadily in time.'' CF counted this as an event, RD did not.
[d]The comment, ''This pair just blinked on,'' was counted as an event by RD, but not by CF.
[e]Observer 5 explained that she was looking for events in which the particles ''flowed'' parallel to one another, instead of just lingered together. Observer 6 stated that the objective was not well posed. We therefore discounted the responses of these observers.

III. RESULTS

The observers' comments were stored in such a way that we could view them without knowing whether the comments were associated with a real or reference set, and resulted in a double blind environment. Initially, we simply read through each of the observers' comments. We looked for, and found, words such as ''lingering'' or ''attracting.'' We also checked whether two or more particles were marked for each comment. In many cases, the observers noted a ''blinking'' of particles, but this was just an artifact due to track breaks. After this initial reading, we used special viewing software to complete our evaluations. This ''viewer'' was also written in Tcl/Tk and C, and was very similar in appearance and functionality to the AMP. The viewer allowed us to play through the movies to see which particles the observers had marked and what comments they had made at different points during the movies. Due to the subjectivity involved in the evaluation of the comments, the authors (RD and CF) evaluated the comments independently in order to provide a consistency check and to aid in the estimation of uncertainties. Table I shows the number of events detected for each movie. In almost all cases, RD's and CF's evaluations agreed, but discrepancies arose when ambiguous wording was used in the comments, and specific examples are noted at the bottom of Table I. Two of the six original observers did not respond in such a way that they could be included in the study, as noted in footnote e of Table I, so, in subsequent discussions, the word ''observers'' will refer only to the four remaining observers.

We assert that the number of events found by the observers depends on three factors: the strength of the interaction between the particles, the total number of particles in the field of view, and the inherent tendency for an observer to find events. In order to quantify this last factor, we assume that pairs of particles represent a stimulus which can trigger an observer to mark a lingering event. The ''strength'' of the stimulus is how strongly the particles are lingering, a concept we will discuss in more detail below. We assume that there is some threshold stimulus at which the response will increase rapidly.

The probability that a given pair will be marked is the observer's response function at a given stimulus level, times the probability of that stimulus level, summed over all possible stimulus levels. We will approximate the response function as a step function with low value λ_1 and high value λ_2. The probability of a marked pair is now just λ_2 times the probability that the stimulus is greater than the crossover value, plus λ_1 times the probability that the stimulus is less than the crossover value.

Let us put this into a more mathematical framework using probability theory. We will use the term ''candidate pair'' to describe a pair of particles that are lingering above the threshold strength level. We will denote the existence of a candidate pair by the letter C, and the presence and absence of pairwise particle interactions by I and N, respectively. The conditional probability that a given pair is a candidate pair is then $\mathcal{P}(C|I)$ and $\mathcal{P}(C|N)$ for systems with and without interactions, respectively. We will denote the marking of a pair by an observer by E. The probability that a pair is marked by an observer, conditioned on whether or not interactions are present, is given by

$$\mathcal{P}(E|I)=\mathcal{P}(E|C\cap I)\mathcal{P}(C|I)+\mathcal{P}(E|C^c\cap I)\mathcal{P}(C^c|I), \quad (1)$$

$$\mathcal{P}(E|N)=\mathcal{P}(E|C\cap N)\mathcal{P}(C|N)+\mathcal{P}(E|C^c\cap N)\mathcal{P}(C^c|N), \quad (2)$$

where a superscript c denotes the complement of the event.

Now we make the following assumptions:

$$\mathcal{P}(E|C\cap I)=\mathcal{P}(E|C\cap N)\equiv\lambda_2, \quad (3)$$

$$\mathcal{P}(E|C^c\cap I)=\mathcal{P}(E|C^c\cap N)\equiv\lambda_1. \quad (4)$$

In other words, as long as the particles are lingering near each other above the threshold level, it does not matter if they are interacting or not; they will still be marked. Define $p_i \equiv \mathcal{P}(C|I)$ and $p_n \equiv \mathcal{P}(C|N)$ as the probability of the formation of a candidate pair conditioned on whether interactions are present or absent, respectively. Then Eqs. (1) and (2) become

$$\mathcal{P}(E|I) = \lambda_2 p_i + \lambda_1 (1 - p_i), \tag{5}$$

$$\mathcal{P}(E|N) = \lambda_2 p_n + \lambda_1 (1 - p_n). \tag{6}$$

We can introduce an excess event statistic ΔE, which expresses the fractional difference in the event probabilities for the interacting and noninteracting cases, as follows:

$$\Delta E = \frac{\mathcal{P}(E|I) - \mathcal{P}(E|N)}{\frac{1}{2}[\mathcal{P}(E|I) + \mathcal{P}(E|N)]}, \tag{7}$$

which, using Eqs. (5) and (6), becomes

$$\Delta E = \frac{p_i - p_n}{\frac{1}{2}(p_i + p_n) + \beta}, \tag{8}$$

where $\beta \equiv ((\lambda_2/\lambda_1) - 1)^{-1}$ quantifies human discrimination. Assuming that $\lambda_2 \geq \lambda_1$ (a person is not more likely to mark noncandidate pairs than candidate pairs), we have $\beta \geq 0$, where a small value of β indicates good discrimination between ''real'' and ''false'' events. We assert that the design of the experiment was such that the discrimination was good, and thus $\beta \approx 0$. We will later check this assertion against the data. By construction, $-2 \leq \Delta E \leq 2$, where a value close to 2 indicates a strong tendency for particles to linger, whereas a value close to -2 indicates a strong tendency for particles to avoid lingering.

Exactly what constitutes a lingering event is undoubtedly different for each observer. However, after careful examination of the movies and comments using the viewer software, we found a fairly good quantitative approximation for the observers' criteria for what constitutes a lingering event by introducing the space and time parameters R and T as follows: if two particles are initially less than $R = 10 \pm 3$ particle radii (5.27 ± 1.58 μm) apart, and are still less than a distance R apart after $T = 100 \pm 50$ frames (13.5 ± 6.8 s), then it was a candidate for a lingering event [18]. The uncertainties indicate the variability in an individual observer's criteria. Therefore, the probabilities p_i and p_n of Eq. (8) are each the product of two different probabilities. The first is the probability, given that two particles are within the field of view and at most a distance R apart in the projected x-y plane (but not overlapping), that they will still be at most a distance R apart in the x-y plane after a time T. This probability is denoted by $\tilde{p}_i$ ($\tilde{p}_n$) for the interacting (noninteracting) case. The second is the probability that another particle will initially be at most a distance R away from a given particle in the x-y plane. The latter probability is given by $\rho(\pi R^2 h - \frac{4}{3}\pi a^3)$ in the low-density limit for both cases, where ρ is the number density of particles, h is the depth of field, and a is the particle radius. We have $\rho = \bar{N}_p / hA$, where A is the field of view area in the x-y plane, and $\bar{N}_p$ is the average number of particles per frame in the field of view, and thus

$$p_i = \tilde{p}_i \bar{N}_i \pi R^2 / A, \tag{9}$$

$$p_n = \tilde{p}_n \bar{N}_n \pi R^2 / A, \tag{10}$$

where we neglected the correction for the volume of a particle, and $\bar{N}_i$ and $\bar{N}_n$ are the average number of particles per frame in the field of view in the interacting and noninteracting cases, respectively. Note that we implicitly assumed in the definition of the lingering probability, $\tilde{p}$, that the pair correlation function $g(r)$ is given by $g(r) = 0$ for overlapping particles, and $g(r) = 1$ otherwise. This is valid, as the volume fraction is very low.

The actual number of events marked in the original and reference data sets will be called E_{orig} and E_{ref}, respectively. We assert that, for a given event probability, both E_{orig} and E_{ref} scale as a single power of $\bar{N}_p$, since we expect observers are looking only at nearest-neighbor pairs, and not at all possible pairs (which would give scaling as $\bar{N}_p^2$). Thus we expect that

$$E_{\text{orig}} = z f(T_{\text{dur}}) \bar{N}_p \mathcal{P}(E|I), \tag{11}$$

$$E_{\text{ref}} = z f(T_{\text{dur}}) \bar{N}_p \mathcal{P}(E|N), \tag{12}$$

where z is the number of nearest-neighbor pairs considered by the observers for each particle, which we take to be of order 1. $f(T_{\text{dur}})$ is some increasing function of the total duration time of the animation T_{dur}, and accounts for the possibility of a candidate pair forming at any time during the animation, i.e., the longer the movie, the more chances there are for lingering events to occur.

Combining the relations for E_{orig}, E_{ref}, p_i and p_n with Eqs. (5) and (6), we obtain

$$E = z\lambda_1 f(T_{\text{dur}}) \bar{N}_p + z(\lambda_2 - \lambda_1) \frac{\pi R^2}{A} f(T_{\text{dur}}) \tilde{p} \bar{N}_p^2 \tag{13}$$

$$\equiv \gamma_1 \bar{N}_p + \gamma_2 \bar{N}_p^2, \tag{14}$$

where E is the number of events detected, and $\tilde{p}$ is either $\tilde{p}_i$ or $\tilde{p}_n$ for interacting and noninteracting particles, respectively. Thus we have

$$\beta = \frac{\pi R^2}{A} \frac{\gamma_1}{\gamma_2} \tilde{p} = (1/\bar{N}_p) \frac{\gamma_1}{\gamma_2} p, \tag{15}$$

where β is as given in Eq. (8). To estimate β, we assumed that $\tilde{p}_i \approx \tilde{p}_n$, then fit to Eq. (14) the average number of events observed and average number of particles per frame corresponding to each of the six different data sets. These data, along with the best fit, are shown in Fig. 5 [19]. From graphical inspection of the error ellipse of the fit ($\Delta\chi^2 = 1$), we find that γ_1/γ_2 can range from -6 to 9. Therefore, since $\bar{N}_p \approx 10$, Eq. (15) gives $\beta/p \approx -0.6$ to 0.9, where p is $p_i \approx p_n$. We therefore see that our assertion that the brain is a good discriminator for the problem at hand, i.e., $\beta \approx 0$, is at least consistent with the data. Setting $\beta = 0$, and inserting

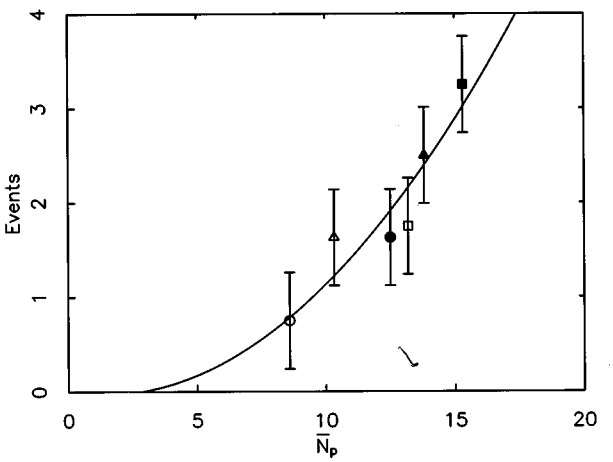

FIG. 5. The average number of lingering events observed as a function of average number of particles per frame $\overline{N}_p$. The open and filled symbols represent real and reference data, respectively. The squares, circles, and triangles correspond to frames 1–350, 351–700, and 701–1050, respectively. The solid curve shows the zero intercept parabola of best fit.

Eqs. (9) and (10) into Eq. (8), we obtain the excess event statistic in terms of $\tilde{p}_l$ and $\tilde{p}_n$:

$$\Delta E_{\text{calculated}} = 2\frac{\overline{N}_l\tilde{p}_l - \overline{N}_n\tilde{p}_n}{\overline{N}_l\tilde{p}_l + \overline{N}_n\tilde{p}_n}, \tag{16}$$

where the common factor of $\pi R^2/A$ has been canceled. Likewise, substituting Eqs. (11) and (12) into Eq. (7), we obtain the excess event statistic in terms of the observed event counts:

$$\Delta E_{\text{observed}} = 2\frac{E_{\text{orig}}/\overline{N}_{\text{orig}} - E_{\text{ref}}/\overline{N}_{\text{ref}}}{E_{\text{orig}}/\overline{N}_{\text{orig}} + E_{\text{ref}}/\overline{N}_{\text{ref}}}, \tag{17}$$

where $\overline{N}_{\text{orig}}$ and $\overline{N}_{\text{ref}}$ are the average number of particles per frame in the original and reference data sets respectively. Diffusion theory gives us $\tilde{p}_l$ and $\tilde{p}_n$, so we can use Eq. (16) to estimate $\Delta E_{\text{observed}}$.

The excess event statistic $\Delta E_{\text{observed}}$ was computed using Eq. (17) with the data shown in Table I for each of the original-reference data set pairs (frame sets), and the results are shown in Table II. Equation (16) suggests that ΔE depends explicitly on $\overline{N}_p$, so we cannot combine the results for different frame sets, because each of the six animations has a different value of $\overline{N}_p$. Thus, we compute ΔE for each data set by averaging over the four observers. $\Delta E_{\text{observed}}$ is then the average of RD's and CF's calculated ΔE's. For each frame set, we treat the variance of ΔE over the volunteers as the random error, and the difference between RD's and CF's scores as a systematic error [20]. Table III shows $\Delta E_{\text{observed}}$, along with the corresponding baseline value, given by Eq. (16) with $\tilde{p}_l = \tilde{p}_n$:

$$\Delta E_{\text{baseline}} = 2\frac{\overline{N}_l - \overline{N}_n}{\overline{N}_l + \overline{N}_n}. \tag{18}$$

This is the expected value of ΔE based solely on differences in number density: the more particles there are in a movie, the more candidate pairs will be expected to form, even when no interactions are present. Any deviation from $\Delta E_{\text{baseline}}$ indicates some sort of interaction between the particles. None of the values for $\Delta E_{\text{observed}}$ were statistically different from the corresponding baseline value.

This result suggests that any observed interparticle lingering in a dilute colloidal system on the time scale of casual observation through a microscope (one minute duration, 50×50 μm^2 field of view) is purely artifactual. Since, as we will show, electrostatic and van der Waals forces are negligible, this lack of lingering might be surprising, because it appears that there should be enhanced lingering due to the increased friction when two suspended particles are in close proximity. The relative importance of hydrodynamic interactions and how much extra lingering the hydrodynamic friction is expected to produce is discussed below.

IV. DISCUSSION

A. Particle interactions

The videotaped particles were approximately 60 μm above the microscope slide, which means that wall-particle hydrodynamic interactions act to reduce the free particle diffusion coefficient by about 1% from the value given by the Einstein-Stokes equation [16]. An advantage of using randomized data sets as controls is that any interaction that affects all particles equally, i.e., particle-wall interactions, will be present in both the real and randomized data. Thus, any observed lingering signal will solely be a result of particle-particle interactions.

The three types of particle-particle interactions present in the system are the attractive van der Waals force $F_{\text{vdW}}(r)$ [21], the repulsive electrostatic force $F_{\text{el}}(r)$ (also known as the double layer force) [22], and hydrodynamic interactions. The first two forces have the forms

TABLE II. Excess event statistic calculated from the data in Table I. The columns marked RD and CF indicate which researcher's scoring was used in the calculation. The range of the excess event statistic is $-2\leqslant\Delta E\leqslant2$, where a value close to 2 indicates a strong tendency for particles to linger, whereas a value close to -2 indicates a strong tendency for particles to avoid lingering.

	Observer 1		Observer 2		Observer 3		Observer 4	
Frame sequence	RD	CF	RD	CF	RD	CF	RD	CF
1–350	−0.88	−0.88	−0.26	−0.26	0.54	−0.53	−0.73	−0.73
351–700	[a]	[a]	0.37	0.37	−0.32	−2.0	−0.93	−0.03
701–1050	−0.77	−0.77	−1.0	−1.0	0.91	0.29	0.67	0.67

[a]No events were marked in both the original and reference data sets.

TABLE III. The average of the excess event statistic given in Table II over the four observers for each of the frame sets is $\Delta E_{\text{observed}}$. The first uncertainty in this result is the random error, and the second is the systematic error. $\Delta E_{\text{baseline}}$ is the expected result from Eq. (16) for $\tilde{p}_l = \tilde{p}_h$. ΔE_{simul} and ΔE_{anal} are the results of the simulation and analytical calculation, respectively.

Frame sequence	$\Delta E_{\text{observed}}$	$\Delta E_{\text{baseline}}$	ΔE_{simul}	ΔE_{anal}
1–350	$(-0.47\pm0.25)\pm0.14$	-0.15	$(-0.042\pm0.011)\pm0.07$	$(-0.053\pm0.004)\pm0.06$
351–700	$(-0.42\pm0.58)\pm0.13$	-0.37	$(-0.267\pm0.011)\pm0.06$	$(-0.277\pm0.004)\pm0.05$
701–1050	$(-0.12\pm0.44)\pm0.08$	-0.29	$(-0.184\pm0.011)\pm0.06$	$(-0.194\pm0.004)\pm0.06$

$$F_{\text{vdW}}(r) = \frac{-32W}{3a(r/a)^3[(r/a)^2-4]^2}, \tag{19}$$

$$F_{\text{el}}(r) = \frac{Q^2}{4\pi\epsilon}\frac{\exp[-(r-2a)/\lambda_D]}{(1+a/\lambda_D)^2}\left(\frac{1}{\lambda_D r}+\frac{1}{r^2}\right), \tag{20}$$

where r is the center to center separation between the spheres, a is the particle radius, Q is the charge on the particles, λ_D is the Debye length, and W is the Hamaker constant, of the order of 10^{-21}–10^{-20} J for polystyrene spheres in water [23]. Later in this paper, the hydrodynamic interaction will be quantified using a diffusivity tensor that varies with particle separation. We will see that, at the length scales of interest, the mean-square separation in the x-y plane between two spheres increases with time t due to diffusive motion approximately as $8D_0(1-\epsilon)t$, where ϵ is a positive number very close to a/r. In the absence of hydrodynamic effects, $\epsilon=0$, so hydrodynamic interactions tend to inhibit the movement of the particles away from each other. The characteristic length scale R_{char} and time scale T_{char} in this system are taken to be the parameters R and T given in Sec. III. The effect of hydrodynamics on the motion of the spheres can be characterized by the ''hydrodynamic drift,'' defined to be how much less the separation increases in time T_{char} due to the presence of hydrodynamic interactions. If the initial separation is R_{char}, then this drift is given by

$$\sqrt{R_{\text{char}}^2+8D_0T_{\text{char}}}-\sqrt{R_{\text{char}}^2+8D_0(1-\epsilon)T_{\text{char}}} \approx (a/R_{\text{char}})\sqrt{D_0T_{\text{char}}} \tag{21}$$

because $R_{\text{char}}^2 \lesssim 8D_0T_{\text{char}}$, where we have neglected factors of the order of 2, and used our approximation for ϵ. Likewise, the drift distances in time T_{char} due to the van der Waals and electrostatic forces are given approximately by $F_{\text{vdW}}(R_{\text{char}})T_{\text{char}}/(6\pi\eta a)$ and $F_{\text{el}}(R_{\text{char}})T_{\text{char}}/(6\pi\eta a)$, respectively. Since the van der Waals force is attractive, while the electrostatic force is repulsive, these distances will be of opposite sign, so we add their magnitudes to obtain our estimate for the importance of these forces. Since our lingering analysis is based on the time dependence of the particle-particle separation, we define a dimensionless number, called the drift ratio Dr, to be the ratio of the extra drift due to hydrodynamic effects to the extra drift due to other forces:

$$Dr = \frac{(a/R_{\text{char}})\sqrt{D_0T_{\text{char}}}}{(|F_{\text{vdW}}(R_{\text{char}})|+|F_{\text{el}}(R_{\text{char}})|)T_{\text{char}}/(6\pi\eta a)}. \tag{22}$$

This dimensionless number quantifies the relative strength of the hydrodynamic interaction with respect to the conservative interactions.

In order to compute Dr, we need estimates for the Debye length and particle charge. We do not independently characterize our specimen, but rather rely on comparison with other experiments, specifically, those of Crocker and Grier [6–8]. From Crocker and Grier's measurements of the interaction potential between colloidal particles in water in a glass cell [6–8], we obtain Debye lengths in the range of 100 to 200 nm [24]. Since Crocker and Grier used ion exchange resin in their sample cell to reduce the water's ionicity, while we did not, we use their measured Debye lengths as an upper bound on the Debye length of our system [25]. These values are consistent with the Debye lengths measured by Kepler and Fraden [23], but much shorter than those of Vondermassen *et al.*, who obtained screening lengths as long as 416 nm [26]. In order to estimate the surface charge, we appeal to charge renormalization theory, which asserts that the surface charge on highly charged spheres saturates at the level where the chemical potential at the surface and in the bulk are equal [27]. This yields a ''renormalized'' charge $Q=Ce(a/\lambda_B)$, where the Bjerrum length $\lambda_B=e^2/(4\pi\epsilon kT)\approx0.72$ nm in water at room temperature, e is the electronic charge, and C is a constant in the range of 4 to 10 [6,8,27]. This gives an estimated particle charge of $3000e-7500e$. While we are confident enough in charge renormalization theory and the results of Crocker and Grier for the purposes of this work, in particular because of their careful discussion of data reduction and analysis, it is clear that further progress calls for better sample characterization.

In order to show that hydrodynamic interactions dominate, we want to find an upper limit on the drift ratio [Eq. (22)], and thus consider values for the length and time scales that tend to decrease the drift ratio. Increasing T_{char} and decreasing R_{char} cause Dr to decrease, so, since our values of R and T from Sec. III have uncertainties associated with them, we choose values for R_{char} and T_{char} statistically close to R and T, but deviating in the directions that decrease Dr. Accordingly, we let R_{char} range from $5a$ to $10a$, and set $T_{\text{char}}=25$ s. Figure 6 shows some curves of constant Dr for intermediate values of charge and Hamaker constant $Q=5000e$ and $W=3\times10^{-21}$ J. We see that for most reasonable choices for the length scale (within 1–2 standard deviations of the optimal value $10a$) and Debye length, the drift ratio is very large. Thus we conclude that electrostatic and van der Waals interactions may be neglected in the analysis, and only hydrodynamic interactions need be considered.

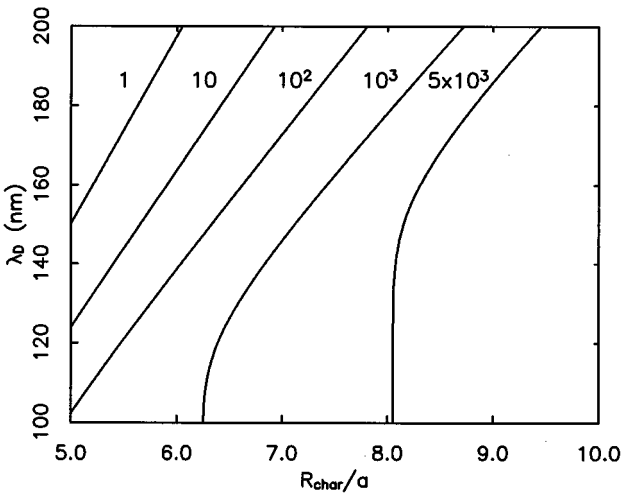

FIG. 6. Contour plot of drift ratio Dr for particle charge $Q=5000e$, Hamaker constant $W=3\times10^{-21}$ J, and characteristic time scale $T_{\text{char}}=25$ s. For reasonable values of the distance scale R_{char} and Debye length λ_D as described in the text, the drift ratio is much larger than 1, showing that hydrodynamic forces are more important than conservative forces in this system over the time and length scales of interest. Varying W and Q within the limits given in the text does not change this plot significantly.

In the next two sections, we find estimates for the lingering probabilities $\tilde{p}_l$ and $\tilde{p}_h$ by integrating the pair probability distribution over the space determined by the lingering criteria discussed earlier. We assume that in each pair, the particles interact hydrodynamically only with each other. Both a computer simulation technique and an analytical perturbation solution are discussed. These results are then used in Eq. (16) to find a theoretical estimate for ΔE, which we compare with the baseline and observed values to answer the question as to whether the enhanced lingering is consistent with results obtained using the aforementioned human stimulus-response formalism.

B. Computer simulations

We start our analysis with the Langevin equation describing the relative motion of two identical spheres in a viscous fluid [21],

$$m\,\frac{d^2\mathbf{r}}{dt^2}=-\mathbf{f}_r(\mathbf{r})\cdot\frac{d\mathbf{r}}{dt}+\mathbf{F}, \tag{23}$$

where m is the mass of the spheres, $\mathbf{r}$ is the relative separation vector between the centers of the spheres, $\mathbf{f}_r(\mathbf{r})$ is the relative friction tensor, and $\mathbf{F}$ is the relative Brownian force. $\mathbf{F}$ is a random force with the properties $\langle\mathbf{F}\rangle=0$ and $\langle\mathbf{F}(t)\mathbf{F}(t+\tau)\rangle=4kT\mathbf{f}_r(\mathbf{r})\,\delta(\tau)$, where $\delta(\tau)$ is the Dirac delta function. If we Taylor expand $\mathbf{f}_r(\mathbf{r})$ to first order about a separation vector $\mathbf{r}(t)$, substitute this into Eq. (23), and solve the resulting differential equation, we obtain [21]

$$\mathbf{r}(t+\Delta t)=\mathbf{r}(t)+\boldsymbol{\nabla}\cdot\mathbf{D}_r(\mathbf{r})\Delta t+\Delta\mathbf{r}(\Delta t), \tag{24}$$

valid for $\Delta t\gg(m/2kT)\,|\mathbf{D}_r(\mathbf{r}(t))|$ where $\mathbf{D}_r=2kT\mathbf{f}_r^{-1}(\mathbf{r}(t))$ is the relative diffusion tensor and $\Delta\mathbf{r}(\Delta t)$ is a random displacement with $\langle\Delta\mathbf{r}(\Delta t)\rangle=0$ and $\langle\Delta\mathbf{r}\Delta\mathbf{r}\rangle=2\mathbf{D}_r(\mathbf{r}(t))\Delta t$. Since $|\mathbf{D}_r|\leqslant2D_0$ for all $\mathbf{r}$, where D_0 is the free single-particle diffusion coefficient, a more strict condition on Δt is $\Delta t\gg(m/kT)\,D_0=(2/9)(a^2\rho/\eta)$, where ρ is the density of the particle. In order for the Taylor expansion to be accurate to first order, we require that the particle configuration not change much over the time step Δt. Thus we must also have $\Delta t\ll a^2/|\mathbf{D}_r|$. Using the upper bound on $|\mathbf{D}_r(\mathbf{r}(t))|$, we find that if $a^2\rho/\eta\ll\Delta t\ll a^2/(2D_0)$, then the necessary conditions on Δt are satisfied.

Batchelor [28] gave the relative diffusion tensor $\mathbf{D}_r$ as

$$\mathbf{D}_r=2D_0[G(\tilde{r})\hat{\mathbf{r}}\hat{\mathbf{r}}+H(\tilde{r})(\boldsymbol{\delta}-\hat{\mathbf{r}}\hat{\mathbf{r}})], \tag{25}$$

where $\boldsymbol{\delta}$ is the identity tensor, $\tilde{\mathbf{r}}=\mathbf{r}/a$, $\tilde{r}=|\tilde{\mathbf{r}}|$, $\hat{\mathbf{r}}=\mathbf{r}/|\mathbf{r}|$, and $G(\tilde{r})$ and $H(\tilde{r})$ are given by

$$G(\tilde{r})=1-\tfrac{3}{2}\tilde{r}^{-1}+\tilde{r}^{-3}-\tfrac{15}{4}\tilde{r}^{-4}+O(\tilde{r}^{-6}), \tag{26}$$

$$H(\tilde{r})=1-\tfrac{3}{4}\tilde{r}^{-1}-\tfrac{1}{2}\tilde{r}^{-3}+O(\tilde{r}^{-6}). \tag{27}$$

These are the far-field form of the equations in the quasistatic approximation, in which inertial terms are neglected and an unbounded medium is assumed [29]. At near contact ($\tilde{r}=2$), these equations no longer hold due to the breakdown of the unbounded medium assumption. However, for $\tilde{r}=2.5$, expressions (26) and (27) agree with more exact results [28] to within 2%, and for $\tilde{r}\geqslant3$ they agree to within 1%, so we will assume they hold for all $\tilde{r}\geqslant2$.

Let us recast Eq. (24) in nondimensional form. Define a characteristic time $\tau=a^2/(2D_0)$. This is the time it takes for the particle separation squared to increase by one particle radius squared. Now define a scaled time $\tilde{t}=t/\tau$. Taking the divergence of the diffusivity tensor, we obtain

$$\boldsymbol{\nabla}\cdot\mathbf{D}_r=15\,\frac{D_0}{a}\left(\frac{a}{r}\right)^5\hat{\mathbf{r}}. \tag{28}$$

Substituting Eqs. (28) and (25) into Eq. (24), along with the scalings for t and $\mathbf{r}$, we obtain

$$\tilde{\mathbf{r}}(\tilde{t}+\Delta\tilde{t})=\tilde{\mathbf{r}}(\tilde{t})+\tfrac{15}{2}\tilde{r}^{-5}\Delta\tilde{t}\hat{\mathbf{r}}+\Delta\tilde{\mathbf{r}}(\Delta\tilde{t}), \tag{29}$$

where $\langle\Delta\tilde{\mathbf{r}}\rangle=0$. For the characteristic length and time scales present in our system, the random Brownian term in this equation dominates over the drift term, but, for completeness, both terms were included in the simulations. If we use a comoving coordinate system where the z axis always points in the direction of the separation vector $\tilde{\mathbf{r}}(\tilde{t})$, then

$$\langle\Delta\tilde{z}\Delta\tilde{z}\rangle=2(1-\tfrac{3}{2}\tilde{z}^{-1}+\tilde{z}^{-3}-\tfrac{15}{4}\tilde{z}^{-4})\Delta\tilde{t}, \tag{30}$$

$$\langle\Delta\tilde{x}\Delta\tilde{x}\rangle=\langle\Delta\tilde{y}\Delta\tilde{y}\rangle=2(1-\tfrac{3}{4}\tilde{z}^{-1}-\tfrac{1}{2}\tilde{z}^{-3})\Delta\tilde{t}, \tag{31}$$

$$\langle\Delta\tilde{x}\Delta\tilde{y}\rangle=\langle\Delta\tilde{x}\Delta\tilde{z}\rangle=\langle\Delta\tilde{y}\Delta\tilde{z}\rangle=0, \tag{32}$$

and the bounds on the scaled time step are $2D_0\rho/\eta\ll\Delta\tilde{t}\ll1$. If there are no hydrodynamic interactions, then $\mathbf{D}_r=2D_0\boldsymbol{\delta}$, and

$$\tilde{\mathbf{r}}(\tilde{t}+\Delta\tilde{t})=\tilde{\mathbf{r}}(\tilde{t})+\Delta\tilde{\mathbf{r}}(\Delta\tilde{t}), \tag{33}$$

where $\langle\Delta\tilde{\mathbf{r}}\rangle=0$, and

$$\langle \Delta\tilde{\mathbf{r}}\Delta\tilde{\mathbf{r}}\rangle = 2\boldsymbol{\delta}\Delta\tilde{t} \tag{34}$$

Equations (29)–(32), and Eqs. (33) and (34) can be used to simulate the trajectory of a particle undergoing Brownian motion with and without hydrodynamic interactions, respectively.

The simulation proceeds as follows. First, an initial separation vector is chosen such that the particles do not overlap, are no more than a distance R apart in the x-y plane, and no more than half the depth of field apart in the z direction. We do not use the full depth of field in this initial separation calculation because, on average, the particles will be near the center of the depth of field. Next, depending on whether interactions are present or not, the appropriate equations are used to simulate the particle's trajectory, using a Gaussian distribution to choose the random deviations $\Delta\tilde{\mathbf{r}}$. The change in the separation vector for each step of the simulation is calculated using the comoving coordinate system, then transformed into a fixed coordinate system using a solid body rotation. If we were to use the fixed coordinate system to calculate the steps, then there would be cross correlations between coordinates, i.e., Eq. (32) would not hold. We used a time step $\Delta\tilde{t}=0.01$, which satisfies the necessary bounds on $\Delta\tilde{t}$, as $2D_0\rho/\eta \approx 10^{-6}$. After a time T, we check to see if the particles are at most a distance R apart in the x-y plane, and at most $h/2$ apart in the z direction, where we used the experimental values for R, T, and h cited earlier. The fractions of particles that satisfy these criteria are $\tilde{p}_i$ and $\tilde{p}_n$ for interacting and noninteracting particles, respectively.

Fifty thousand trajectories were simulated for the interacting and noninteracting cases, which yielded $\tilde{p}_i = (0.267 \pm 0.002) \pm 0.14$ and $\tilde{p}_n = (0.240 \pm 0.002) \pm 0.14$. The first uncertainty is the random error of the results, i.e., the error in the integration when using a given set of lingering criteria. The second uncertainty is the systematic error, i.e., the range over which $\tilde{p}$ can vary when the quantities R, T, and h vary within their individual uncertainties. Using Eq. (16), we obtain the excess event statistic expected from the simulations, ΔE_{simul} [30], which is shown in Table III. Below, we calculate $\tilde{p}_i$ and $\tilde{p}_n$ using analytical methods.

C. Analytical approximations

In this section, we use a perturbation technique to solve approximately the probability conservation equation when hydrodynamic interactions are present, and use the solution to obtain another estimate for $\tilde{p}_i$ and $\tilde{p}_n$. We start with the Smoluchowski equation for the pair probability distribution $P(\mathbf{r},t)$, with a tensor diffusivity $\mathbf{D}_r$ [31]:

$$\frac{\partial}{\partial t} P(\mathbf{r},t) = \mathcal{L}P(\mathbf{r},t), \tag{35}$$

with initial condition [32]

$$P(\mathbf{r},0) = \delta(\mathbf{r}-\mathbf{r}_0), \tag{36}$$

where $\mathbf{r}$ is the vector from one particle's center to the other, $\mathbf{r}_0$ is the initial separation vector, $\delta(\mathbf{r})$ is the Dirac delta function, t is the time, and $\mathcal{L}$ is a scalar linear operator given by

$$\mathcal{L} = \boldsymbol{\nabla}\cdot\mathbf{D}_r\cdot\boldsymbol{\nabla}. \tag{37}$$

Note that if there are no interactions, then $\mathbf{D}_r = 2D_0\boldsymbol{\delta}$ and $\mathcal{L} = 2D_0\nabla^2$, which, when substituted into Eq. (35), yields the usual diffusion equation. D_0 is the single-particle free diffusion coefficient.

We can write $\mathcal{L} = \mathcal{L}_0 + \mathcal{L}_1$, where $\mathcal{L}_0 = 2D_0\nabla^2$, and $\mathcal{L}_1 = \boldsymbol{\nabla}\cdot\mathbf{T}\cdot\boldsymbol{\nabla}$, where

$$\mathbf{T} = \mathbf{D}_r - 2D_0\boldsymbol{\delta} \tag{38}$$

$$= 2D_0[(G(\tilde{r})-1)\hat{\mathbf{r}}\hat{\mathbf{r}} + (H(\tilde{r})-1)(\boldsymbol{\delta}-\hat{\mathbf{r}}\hat{\mathbf{r}})] \tag{39}$$

is the hydrodynamic interaction tensor [33], and $G(\tilde{r})$, $H(\tilde{r})$ are given by Eqs. (26) and (27). This gives

$$\mathcal{L}_1 = \frac{2D_0}{r^2}\frac{\partial}{\partial r}\left[(G(\tilde{r})-1)r^2\frac{\partial}{\partial r}\right] + 2D_0\frac{H(\tilde{r})-1}{r^2\sin\theta}\frac{\partial}{\partial\theta}\left[\sin\theta\frac{\partial}{\partial\theta}\right] + 2D_0\frac{H(\tilde{r})-1}{r^2\sin^2\theta}\frac{\partial^2}{\partial\phi^2}. \tag{40}$$

A formal solution to Eq. (35) is

$$P(\mathbf{r},t) = e^{(\mathcal{L}_0+\mathcal{L}_1)t}\delta(\mathbf{r}-\mathbf{r}_0), \tag{41}$$

while the solution to the unperturbed (noninteracting) problem ($\mathcal{L}_1 = 0$) is

$$P_B(\mathbf{r},t) = e^{\mathcal{L}_0 t}\delta(\mathbf{r}-\mathbf{r}_0) \tag{42}$$

$$= \frac{1}{(8\pi D_0 t)^{3/2}}\exp[-|\mathbf{r}-\mathbf{r}_0|^2/(8D_0t)]. \tag{43}$$

We can expand the exponential in Eq. (41) as follows [34]:

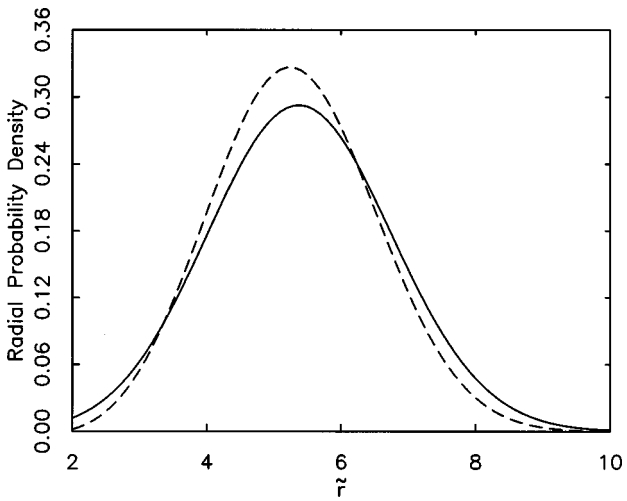

FIG. 7. The radial pair probability distribution for $\tilde{t}=1$ and an initial separation of five particle radii. The dashed line shows the result with hydrodynamic interactions present [$P(\mathbf{r},t)$ integrated over angular variables, i.e., $\int P(\mathbf{r},t)r^2 d\Omega$], and the solid line shows the result without hydrodynamic interactions present [$P_B(\mathbf{r},t)$ integrated over angular variables]. $\tilde{r}$ and $\tilde{t}$ are the scaled variables described in the text.

$$e^{(\mathcal{L}_0+\mathcal{L}_1)t}=e^{\mathcal{L}_0 t}+\int_0^t e^{(\mathcal{L}_0+\mathcal{L}_1)(t-s)}\mathcal{L}_1 e^{\mathcal{L}_0 s}ds. \quad (44)$$

Substituting Eq. (44) into Eq. (41), and using Eq. (42), we obtain

$$P(\mathbf{r},t)=P_B(\mathbf{r},t)+\int_0^t e^{(\mathcal{L}_0+\mathcal{L}_1)(t-s)}\mathcal{L}_1 P_B(\mathbf{r},s)ds. \quad (45)$$

Now we make the approximations

$$e^{(\mathcal{L}_0+\mathcal{L}_1)(t-s)}\approx 1+(\mathcal{L}_0+\mathcal{L}_1)(t-s), \quad (46)$$

$$P_B(\mathbf{r},s)\approx P_B(\mathbf{r},t)+\mathcal{L}_0 P_B(\mathbf{r},t)(s-t), \quad (47)$$

where we used $(\partial/\partial t)P_B=\mathcal{L}_0 P_B$ in Eq. (47). The validity of these approximations will be determined *a posteriori* by looking at the relative size of the resulting perturbation. After substituting Eqs. (46) and (47) into Eq. (45), and evaluating the integral, we obtain the following expansion:

$$P(\mathbf{r},t)\approx P_B(\mathbf{r},t)+t\mathcal{L}_1 P_B(\mathbf{r},t)+\tfrac{1}{2}t^2([\mathcal{L}_0,\mathcal{L}_1]+\mathcal{L}_1^2)P_B(\mathbf{r},t), \quad (48)$$

where the next term is $O(t^3[\mathcal{L}_0,[\mathcal{L}_0,\mathcal{L}_1]]P_B)$. In this work, we use only the first correction term, $t\mathcal{L}_1 P_B(\mathbf{r},t)$. Figure 7 shows how the probability distribution is altered by the presence of hydrodynamic interactions. One can see that, in the presence of hydrodynamic interactions, the most probable pair separation distance increases more slowly with time, and the separation distance has less chance of exhibiting a large deviation from the most probable value. This suggests that enhanced lingering is taking place. We see that, for the time and distance scales involved in this work, the second term in this expansion is a small correction to the unperturbed solution, which suggests that approximations (46) and (47) are valid.

To obtain the explicit dependence of $P(\mathbf{r},t)$ on the spherical coordinates, we expand $|\mathbf{r}-\mathbf{r}_0|$ as

$$|\mathbf{r}-\mathbf{r}_0|^2=r^2+r_0^2-2rr_0\sin\theta\,\sin\theta_0\cos(\phi-\phi_0)-2rr_0\cos\theta\,\cos\theta_0, \quad (49)$$

and write $P_B(\mathbf{r},t)$ as

$$P_B(r,r_0,\theta,\theta_0,\phi,\phi_0,t)=\frac{1}{(8\pi D_0 t)^{3/2}}\exp\left[-\frac{r^2+r_0^2-2rr_0\sin\theta\,\sin\theta_0\cos(\phi-\phi_0)-2rr_0\cos\theta\,\cos\theta_0}{8D_0 t}\right]. \quad (50)$$

The quantity $\tilde{p}_t-\tilde{p}_n$ for a given initial separation $\mathbf{r}_0$ is the integral of $P(\mathbf{r},t)-P_B(\mathbf{r},t)\approx t\mathcal{L}_1 P_B(\mathbf{r},t)$ over $\mathbf{r}$ within a cylinder of dimensions as given in Secs. II and III: height $h=20.4a$ and radius $R=10a$. Since the system is invariant with respect to rotations in ϕ, this probability cannot depend on ϕ_0, so we take $\phi_0=0$. To obtain the total change in probability, we average $\tilde{p}_t-\tilde{p}_n$ over all initial separation vectors $\mathbf{r}_0$ falling within the cylinder given above in which the particles do not overlap.

The last term in $\mathcal{L}_1$ [Eq. (40)] makes no contribution to this integral. This can be seen by noting that this operator forms an exact differential with respect to ϕ when acting on P_B. We may do the integral over ϕ immediately, which gives a term proportional to $(\partial/\partial\phi)P_B]_0^{2\pi}$, which vanishes. Therefore, we only need the first two terms of $\mathcal{L}_1$, which we denote by $\mathcal{L}_1'$:

$$\mathcal{L}_1'\equiv\frac{2D_0}{r^2}\frac{\partial}{\partial r}\left[(G(\tilde{r})-1)r^2\,\frac{\partial}{\partial r}\right]+2D_0\frac{H(\tilde{r})-1}{r^2\sin\theta}\frac{\partial}{\partial\theta}\left[\sin\theta\,\frac{\partial}{\partial\theta}\right]. \quad (51)$$

Since $\mathcal{L}_1'$ does not depend on ϕ, we may do the integral of P_B over ϕ first, then apply $t\mathcal{L}_1'$. Thus we have that

$$\begin{aligned}\int_0^{2\pi} t\mathcal{L}_1 P_B(r,r_0,\theta,\theta_0,\phi,t)d\phi &= t\mathcal{L}_1'\int_0^{2\pi} P_B(r,r_0,\theta,\theta_0,\phi,t)d\phi\\ &= t\mathcal{L}_1'\left[\frac{2\pi}{(8\pi D_0 t)^{3/2}}\exp\left(-\frac{r^2+r_0^2-2rr_0\cos\theta\,\cos\theta_0}{8D_0 t}\right)I_0\left(\frac{2rr_0\,\sin\,\theta\,\sin\,\theta_0}{8D_0 t}\right)\right]\\ &\equiv F(r,r_0,\theta,\theta_0,t),\end{aligned} \quad (52)$$

where $I_0(x)$ is a modified Bessel function of the first kind, and we have introduced the function F.

The natural coordinate system for this calculation of $\tilde{p}_t$ is cylindrical coordinates, so we must transform the spherical variables r,θ into cylindrical variables ρ, z using

$$r=\sqrt{\rho^2+z^2}, \quad (53)$$

$$r_0=\sqrt{\rho_0^2+z_0^2}, \quad (54)$$

$$\theta=\arctan\frac{\rho}{z}, \quad (55)$$

$$\theta_0=\arctan\frac{\rho_0}{z_0}. \quad (56)$$

The final result for the difference in lingering probability between the interacting and noninteracting cases is then

$$\tilde{p}_l-\tilde{p}_h=\frac{2\pi}{\pi R^2 h-\frac{4}{3}\pi(2a)^3}\int_{G(z)}^{R}\int_{G(z_0)}^{R}\int_{-h/2}^{h/2}\int_{-h/2}^{h/2}F\left(\sqrt{\rho^2+z^2},\sqrt{\rho_0^2+z_0^2},\arctan\frac{\rho}{z},\arctan\frac{\rho_0}{z_0},T\right)\rho\rho_0 dz\, dz_0\, d\rho\, d\rho_0, \tag{57}$$

where $F(r,r_0,\theta,\theta_0,t)$ is defined in Eq. (52), R and T are the lingering distance and time specified earlier, h is the depth of field, a is the radius of the particle, and $G(z)\equiv\sqrt{(2a)^2-z^2}$ for $|z|\leqslant 2a$ and is zero otherwise. The factor $\pi R^2 h-4/3\,\pi(2a)^3$ arises from the averaging with respect to $\mathbf{r}_0$ over the cylindrical volume discussed earlier exterior to two nonoverlapping spheres of radius a. Replacing $F(r,r_0,\theta,\theta_0,t)$ in Eq. (57) by $\int_0^{2\pi}P_B(r,r_0,\theta,\theta_0,\phi,t)d\phi$ yields an expression for $\tilde{p}_h$.

The integral of Eq. (57) was evaluated numerically using the software package MATHEMATICA [35]. We only required an accuracy of two significant figures for $\Delta\tilde{p}\equiv\tilde{p}_l-\tilde{p}_h$ and three for $\tilde{p}_h$ in order to keep computation times from being prohibitive. This gave $\tilde{p}_h=(0.242\pm0.001)\pm0.14$ and $\Delta\tilde{p}=(0.025\pm0.001)\pm0.004$, which yielded $\tilde{p}_l=(0.267\pm0.001)\pm0.14$, where the uncertainties are to be interpreted as described at the end of Sec. IV B. Using Eq. (16), we obtain the excess event statistic expected from the analytical work ΔE_{anal}, which is shown in Table III. The values obtained for the excess lingering probability $\Delta\tilde{p}$ from analytical methods are in excellent agreement with the simulation results. However, this good agreement is somewhat fortuitous, as other choices of R, T, and h can lead to a discrepancy of $\approx 30\%$ in the value of $\Delta\tilde{p}$.

One can see from Table III that for each of the animations, ΔE_{anal} and ΔE_{simul} are in good agreement with each other, and are both statistically consistent with $\Delta E_{\text{observed}}$. Likewise, $\Delta E_{\text{observed}}$ is not statistically significantly different from the corresponding $\Delta E_{\text{baseline}}$. Our results are thus compatible with the conclusion that all observed lingering is artifactual in origin.

D. Can the lingering signal be detected?

The difference between $\Delta E_{\text{baseline}}$ and the values of ΔE calculated from the simulation and analytical work is ≈ 0.1. The error in $\Delta E_{\text{observed}}$ is ≈ 0.4. Thus, to reduce the error in the observed results enough to resolve the expected lingering signal, one would need about 16 times more observers, i.e., on the order of a hundred observers. This type of large-scale study was beyond our resources, but we have shown that the expected lingering effect is too weak to be perceived by one individual looking through a microscope for a few seconds, as consistent with our observations.

V. CONCLUSIONS

The dominant interactions in this dilute colloidal system on the length and time scales discussed are hydrodynamic in origin, and thus any attempt to quantify them must incorporate the temporal dimension. Detection methods that are based on purely static quantities such as the static structure factor are of no use. We have described a ''digital'' microscope that unites the fields of light microscopy with that of computing, which allows one to probe quantities that depend on dynamical information. In a double blind experiment, we determined that casual observation of a dilute colloidal system under a microscope is not sufficient to detect hydrodynamic pairwise interparticle lingering effects. Any lingering that appears to be present is solely due to random thermal motion and projection effects. The expected degree of lingering calculated using computer simulations and analytical techniques is consistent with the results obtained using human observers [36].

This observational technique is not sensitive enough to detect hydrodynamic interaction on the length and time scales in this work (5 μm and 10 s, respectively), and thus the traditional purely numerical approach to quantifying the interaction is more appropriate. However, the observational technique could be used as an exploratory tool in helping to determine if an observed interaction warrants further numerical study, or if it is simply an artifact. In addition, the brain's superior spatial-temporal pattern recognition capabilities could be exploited by setting observers free on data, asking them only to look for examples of ''unusual'' lingering events. If these ''rare'' events were then proven to be nonartifactual by use of the described backgrounding technique, then this would provide an impetus for further study. An example of such a ''rare'' event was observed by one of us (C.F.), in which one particle appeared to undergo Brownian motion confined to a small region surrounding another particle that was adhered to one of the glass surfaces. This ''orbiting'' particle was subsequently disassociated from the fixed particle by a ''collision'' with a third particle. The exact physical mechanism by which this occurred is unknown, and, if nonartifactual, serves as an example of the new types of interaction phenomena that might be discovered using the observation technique.

This digital microscope could also be used in other areas of interest to colloidal scientists. Researchers could develop new statistics to quantify correlated colloidal motion by asking the human observers to find instances of multiparticle lingering. Their comments could be very helpful in determining what types of parameters would be most efficient in describing multiparticle lingering. Furthermore, it may be possible to probe interactions that occur on different time and distance scales by adjusting the animation parameters, such as animation frame rate and field of view, to reflect these scales.

ACKNOWLEDGMENTS

We would like to thank Becky Schirato for help with sample preparation and taking the video data, and Brendan Plapp, Eberhard Bodenschatz, and Rolf Ragnarsson for help with the video digitization. The authors had many helpful

discussions with Hector Abruna, James Alexander, Zsofia Franck, Frank Hicks, Donald Koch, Katherine Kollins, Sarah Peach, Robert Polak, and Thomas Van Vechten. We appreciate the help of our observers: Krishnamachari Badrinarayan, Tatjana Curcic, Alexander Khein, Andone Lavery, Thomas Metcalf, and Mohammad Rezaei. We are also grateful to Brian Kelley, Anthony Reeves, Anthony Bretscher (for use of microscope), and Nicholas Szabo for assistance. R. D. wishes to acknowledge financial support from the National Science Foundation. Additional financial support was provided by the National Science Foundation through Grant No. DMR-9320910, and through MRL Central Facilities at the Materials Science Center at Cornell University (DMR-9121654).

[1] B. S. Schirato, M.S. thesis, Cornell University, 1995.

[2] D. Cannell (in a private communication relating his own direct observations) and B. Ackerson (in a private communication describing video microscopy data due to N. Ise).

[3] C. Cheung, Y. H. Hwang, X.-l. Wu, and H. J. Choi, Phys. Rev. Lett. **76**, 2531 (1996).

[4] Scientists have been interested for many years in the visual interpretation of data, albeit in a different context than in the present work. High-energy experimentalists employed human ''scanners'' to search through large numbers of bubble chamber photographs for decay events [A. G. Frodesen, O. Skjeggestad, and H. Tofte, *Probability and Statistics in Particle Physics* (Universitetsforlaget, Bergen, 1979)]. Such methods have a long tradition in biology. For example, in a recent paper, naive observers were used to determine the size distribution of certain fluorescently labeled cellular structures [S. Henderson, R. Allsopp, D. Spector, S.-S. Wang, and C. Harley, J. Cell Biol. **134**, 1 (1996)].

[5] B. S. Schirato and C. Franck, Rev. Sci. Instrum. **67**, 2549 (1996).

[6] J. C. Crocker and D. G. Grier, Phys. Rev. Lett. **73**, 352 (1994).

[7] J. C. Crocker and D. G. Grier, Phys. Rev. Lett. **77**, 1897 (1996).

[8] J. C. Crocker and D. G. Grier, J. Colloid Interface Sci. **179**, 298 (1996).

[9] Central Scientific has been known to change the specifications on its latex spheres while keeping the same stock number.

[10] A. Einstein, Ann. Phys. (N.Y.) **17**, 549 (1905).

[11] The controlling software was written by Rolf Ragnarsson, Physics Dept., Cornell University.

[12] Brendan Plapp, Cornell University, discovered that for unknown reasons, the digitized pixels produced by the imaging system were generally smaller in the horizontal direction by 2.5%. He included instructions in the digitization software that expanded the horizontal scale of the pixels by 2.5% to correct for this. However, after the experiment had already been completed, it was found that the anomalous digitization behavior had inexplicably not occurred with our images, and therefore the correction resulted in slightly distorted images. This led to a slightly different pixel conversion scale in the horizontal and vertical directions, but is not expected to affect the results in any way.

[13] A. P. Reeves, IEEE Software **8** (6), 51 (1991).

[14] W. K. Pratt, *Digital Image Processing* (Wiley, New York, 1978), Chap. 16.

[15] A. P. Reeves (private communication).

[16] L. P. Faucheux and A. J. Libchaber, Phys. Rev. E **49**, 5158 (1994).

[17] The filter used here is very similar to the Schmidt trigger of electronic circuitry. The Schmidt trigger responds at a certain threshold level, and stays high until the input voltage drops below a certain level that is lower than the triggering voltage [J. Millman and A. Grabel, *Microelectronics* (McGraw-Hill, New York, 1987), pp. 679–683]. This hysteresis gives a certain level of noise immunity. What we are employing is a ''noncausal'' Schmidt trigger, as it uses information from the entire time-varying signal.

[18] An ''unreasonable'' choice for these lingering criteria can lead to assumptions (3) and (4) becoming invalid. For example, one could make the criteria to be that the particles must be initially less than 1000 radii apart and are still so after ten frames. Here, $p_i \approx p_n \approx 1$ and $p_i - p_n \approx 0$ because the vast majority of pairs will satisfy these criteria, and the range of the interactions is much less than 1000 particle radii. This would give $\mathcal{P}(C) = 1$, and then Eq. (3) is equivalent to the statement that $\mathcal{P}(E|I) = \mathcal{P}(E|N)$, which is not something we want to assume *a priori*. If very strict lingering criteria are chosen so that $\mathcal{P}(C) \approx 0$, then analogous reasoning shows that Eq. (4) leads to a contradiction. Since the observers seem to have chosen a lingering criteria for which $\mathcal{P}(C) \approx O(0.1)$, Eqs. (3) and (4) are probably reasonable assumptions.

[19] The six data points shown in Fig. 5 and their uncertainties were computed as follows. For each of the six animations given in Table I, we averaged together the eight event counts (four observers with RD's and CF's counts for each observer). The preliminary uncertainty associated with the average event count in a given animation was determined by first averaging together RD's and CF's event counts for each observer, then finding the standard deviation of the mean of these average event counts associated with the four observers of the animation. The final uncertainty was computed by averaging together each of the six standard deviations associated with the mean event counts of the six animations. This uncertainty was used for each of the data points.

[20] The uncertainties in $\Delta E_{\text{observed}}$ were computed as follows. For each data set, we obtained values for the excess event statistic by averaging ΔE over the four volunteers. The standard deviations of the two means independently derived from RD's and CF's scorings were then averaged in quadrature to obtain a conservative estimate of the random error in $\Delta E_{\text{observed}}$. The systematic error was simply taken to be half the difference between CF's and RD's values for the excess event statistic.

[21] W. B. Russel, D. A. Saville, and W. R. Schowalter, *Colloidal Dispersions* (Cambridge University Press, Cambridge, England, 1989).

[22] M. Medina-Noyola and D. A. McQuarrie, J. Chem. Phys. **73**, 6279 (1980).

[23] G. M. Kepler and S. Fraden, Phys. Rev. Lett. **73**, 356 (1994).

[24] In Ref. [7], Crocker and Grier made measurements of the Debye length in systems with both confined and unconfined geometries. We consider the value obtained for their unconfined geometry, $\lambda_D = 100$ nm, to be more relevant to our work. In Ref. [8], they obtained a Debye length of 320 nm, but did not specify the height of their sample cell.

[25] Crocker and Grier argue that the reduction of the measured Debye length below that of pure water (approximately 940 nm) is due to ions leaching out of the glass walls at a constant rate [7]. Since our sample volume is much larger than that used by other workers, but the exposed glass surface area is comparable, one wonders if this ion leaching would have less of an effect on our sample, and thus invalidate the claim that these other workers' results have any bearing on our system. However, it appears that there are also other factors at work in determining the ionicity, as Crocker and Grier have measured similar Debye lengths in cells with an order of magnitude different surface to volume ratio [6,7]. Thus it appears that the ionicity is somewhat independent of the dimensions of the system.

[26] K. Vondermassen, J. Bongers, A. Mueller, and H. Versmold, Langmuir **10**, 1351 (1994).

[27] S. Alexander, P. M. Chaikin, P. Grant, G. J. Morales, and P. Pincus, J. Chem. Phys. **80**, 5776 (1984).

[28] G. K. Batchelor, J. Fluid Mech. **74**, 1 (1976).

[29] After the present work was completed, Crocker found that the Batchelor diffusivity tensor [Eq. (25)] is quantitatively consistent with the variance of the distribution of displacements that two 0.97-μm-diameter spheres in water undergo during a 16.7-ms interval [J. C. Crocker, J. Chem. Phys. **106**, 2837 (1997)]. Due to this short time scale, the spheres in Crocker's experiment have an effectively constant diffusivity during the taking of each data point. In the present paper, we consider displacements that occur over much larger time scales, and thus the particles sample a larger domain of separation vectors during the diffusion process.

[30] The uncertainties in ΔE_{simul} were computed as follows. $\tilde{p}_l$ and $\tilde{p}_n$ are strongly correlated, but $\tilde{p}_l - \tilde{p}_n$ seems to be only weakly dependent on $\tilde{p}_n$ for the parameters relevant to this work. Thus we treated $\tilde{p}_l - \tilde{p}_n$ and $\tilde{p}_n$ as the independent variables, and calculated the random and systematic errors in ΔE_{simul} according to the usual error propagation techniques. The same method was used to compute the uncertainties in ΔE_{anal}, which is discussed later in the text.

[31] B. U. Felderhof and R. B. Jones, Physica A **119**, 591 (1983).

[32] For the case of two hard spheres, the probability flux should also vanish at contact $(r = 2a)$, or $\mathbf{n} \cdot \mathbf{D}_r \cdot \boldsymbol{\nabla} P(r = 2a) = 0$, where $\mathbf{n}$ is the surface normal. This requirement was neglected, because for the length scales of interest, it would not change the probability distribution significantly, as can be seen from Fig. 7.

[33] G. T. Evans and C. P. James, J. Chem. Phys. **79**, 5553 (1983).

[34] J.-P. Hansen and I. R. McDonald, *Theory of Simple Liquids* (Academic, London, 1991), p. 245.

[35] MATHEMATICA version 2.2, Wolfram Research, Inc., Champaign, IL, 1995.

[36] It should be noted that under certain conditions, the Sogami-Ise theory of colloidal interactions [I. Sogami and N. Ise, J. Chem. Phys. **81**, 6320 (1984)] predicts an attractive force between two like charged colloidal particles at separations of a few particle radii. Further, Crocker and Grier [7] found experimentally that, for certain sample cell geometries, pairs of colloidal particles experience an attractive force. We do not feel that either of these possible attractive forces was present in our system, but this does not mean that other workers that have noticed lingering among colloidal particles are not seeing some evidence of these attractive interactions.